ACS Catalysis

Research Article

pubs.acs.org/acscatalysis

Hybrids of a Ruthenium(II) Polypyridyl Complex and a Metal Oxide Nanosheet for Dye-Sensitized Hydrogen Evolution with Visible Light: Effects of the Energy Structure on Photocatalytic Activity

Kazuhiko Maeda,*[,†] Go Sahara,[†] Miharu Eguchi,[‡,§,∥] and Osamu Ishitani[†]

[†]Department of Chemistry, Graduate School of Science and Engineering, Tokyo Institute of Technology, 2-12-1-NE-2 Ookayama, Meguro-ku, Tokyo 152-8550, Japan

[‡]Graduate School of Pure and Applied Sciences, University of Tsukuba, 1-1-1 Tennodai, Tsukuba, Ibaraki 305-8571, Japan

[§]Precursory Research for Embryonic Science and Technology Science and Technology Agency (JST), 4-1-8 Honcho Kawaguchi, Saitama 332-0012, Japan

Supporting Information

ABSTRACT: Hybrid materials consisting of a ruthenium(II) polypyridyl complex and a Dion–Jacobson type perovskite oxide nanosheet were studied as photocatalysts for dye-sensitized H_2 evolution under visible light with respect to the energy structure of the hybrids. Three Ru(II) complexes, $Ru^{II}\{(4,4'\text{-}X_2\text{-bpy})_2(4,4'\text{-}(CH_2PO_3H_2)_2\text{-bpy})\}$ (X = H, CH_3, CF_3; bpy = 2,2′-bipyridine), were used as redox photosensitizers. $HCa_{2-x}Sr_xNb_3O_{10}$ ($0 \le x \le 2$) and $HCa_2Nb_{3-y}Ta_yO_{10}$ ($0 \le y \le 1.5$) nanosheet aggregates, having a tunable conduction band potential (E_{CB}), were employed as the building block. Nanosheets that possess more negative E_{CB} value were found to be preferable for the dye-sensitized H_2 evolution, unless electron injection from the excited-state sensitizer to the conduction band of a nanosheet is hindered. Among the combinations tested, the highest activity was obtained when an $HCa_2Nb_3O_{10}$ nanosheet was sensitized by $Ru^{II}\{(4,4'\text{-}(CH_3)_2\text{-bpy})_2(4,4'\text{-}(CH_2PO_3H_2)_2\text{-bpy})\}$, exhibiting a maximum apparent quantum yield of ca. 10% at 460 nm and a turnover number of ca. 3800 (for 20 h). This study highlighted that it is possible to maximize the performance of dye-sensitized H_2 evolution on a sensitizer/semiconductor hybrid by refining the E_{CB} value of a semiconductor and the oxidation potential of the excited state of a photosensitizer.

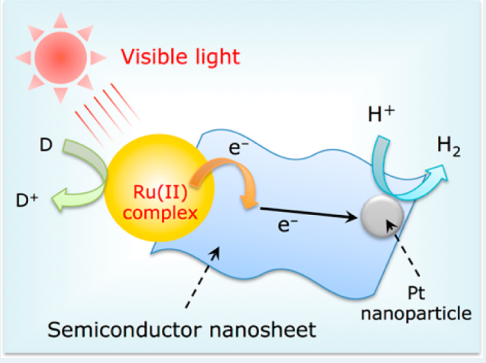

KEYWORDS: *artificial photosynthesis, heterogeneous photocatalysis, layered materials, light energy conversion, water splitting*

1. INTRODUCTION

Catalytic production of hydrogen from water driven by sunlight is of particular importance in recent years from the standpoint of artificial photosynthesis.[1−7] Dye-sensitized hydrogen evolution using a wide-gap semiconductor combined with a redox photosensitizer (e.g., Ru(II) polypyridyl complexes) has long been studied as a potential means of solar-to-fuel conversion,[8−26] since Gerischer introduced the basic principle of spectral sensitization.[27] The mechanism of this reaction is depicted in Scheme 1. Under irradiation of light with energy greater than or equivalent to the energy gap of a sensitizer, the sensitizer undergoes photoexcitation, followed by electron injection to the conduction band of a semiconductor adjacent to the sensitizer. The injected electrons move to catalytically active sites (e.g., nanoparticulate Pt) existing on the semiconductor surface, thereby reducing protons to release H_2. The oxidized sensitizer (i.e., electron-deficient state) is reduced by an electron donor to get back to the ground state.

Certain layered metal oxides are known to undergo exfoliation by reaction with bulky base molecules, producing unilamellar colloids that are so-called nanosheets.[28−37] Because metal oxide nanosheets have a nanosized thickness and lateral dimensions ranging from several hundreds of nanometers to a few micrometers, they are regarded as two-dimensional nanocrystals, and have been employed as heterogeneous photocatalysts.[20−22,32,35−37] Our group has focused on metal oxide nanosheets and nanoscrolls as the building block for dye-sensitized H_2 evolution.[20−22] $H_4Nb_6O_{17}$ nanoscroll and $HCa_2Nb_3O_{10}$ nanosheet, produced from the lamellar niobates by chemical exfoliation with tetra-*n*-butylammonium hydroxide (TBAOH) and concomitant reassembling with HCl, both exhibit higher performance than the lamellar material and a conventional TiO_2, when they are combined with a $Ru(bpy)_3^{2+}$ (bpy = 2,2′-bipyridine) complex as a sensitizer. $HCa_2Nb_3O_{10}$ nanosheet was further studied in order to explore the relationship between catalyst structure and activity. Using a $Ru(bpy)_2(4,4'\text{-}(PO_3H_2)_2bpy)^{2+}$ sensitizer, the rate of sensitized H_2 production was shown to be largely insensitive to structural

Received: September 29, 2014
Revised: February 4, 2015
Published: February 5, 2015

DOI: 10.1021/acscatal.5b00040
ACS Catal. 2015, 5, 1700−1707

Scheme 1. Schematic Illustration of H_2 Evolution from Water Using a Wide-Gap Nanosheet Semiconductor and and a Ru(II) Complex Sensitizer under Visible Light

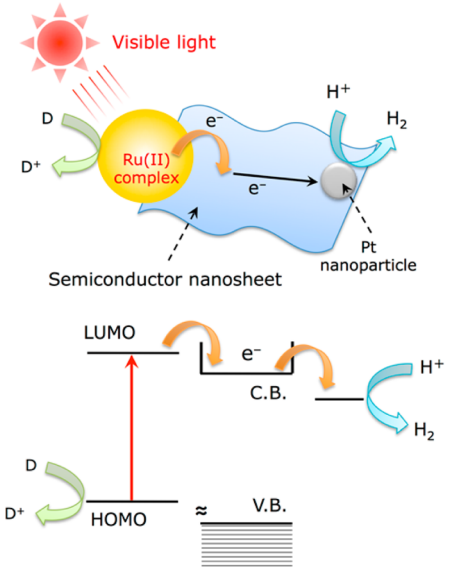

properties, including in-plane crystallinity of the sheet, specific surface area, and the size of lateral dimensions.[22] As can be seen in Scheme 1, it is expected that the H_2 evolution efficiency will be influenced by the energy structure of both sensitizer and semiconductor. More specifically, it is considered that the LUMO level of a sensitizer and the conduction band potential of a semiconductor are both important factors affecting the activity, as they function as the interface of electron transfer. Despite the importance of such energy structures, there have been very few that examine the energy structure effect in detail.

In this study, we systematically investigated the effects of energy structures of a sensitizer/semiconductor composite. We have very recently developed Dion–Jacobson type perovskite nanosheets of $HCa_{2-x}Sr_xNb_3O_{10}$ ($0 \le x \le 2$) and $HCa_2Nb_{3-y}Ta_yO_{10}$ ($0 \le y \le 1.5$), which have tunable conduction band potentials and very high apparent quantum yields (~80% at 300 nm) for H_2 evolution from an aqueous methanol solution under band gap irradiation.[37] The precisely controlled conduction band potential of these materials would be of interest for use as a building block for dye-sensitized H_2 evolution. Factors affecting photocatalytic activities are discussed on the basis of energy structures. The specific surface areas and band gaps of the nanosheet aggregates are summarized in Table 1, and the detailed characterization data of these nanosheets can be found in our previous paper.[37]

2. RESULTS AND DISCUSSION

2.1. Immobilization of Ru(II) Complexes onto Nanosheets. In this work, we synthesized three different Ru(II) polypyridyl complexes as visible-light sensitizers (Figure 1). The spectroscopic and electrochemical properties are summarized in Table 2. The adsorption of these complexes onto Pt-loaded $HCa_{2-x}Sr_xNb_3O_{10}$ nanosheets was performed by dispersing the aggregated nanosheet solid in an aqueous solution dissolving a Ru(II) complex (8.0 μmol g^{-1}). It was confirmed by means of UV–visible spectroscopy that the dissolved Ru(II) complex was almost quantitatively adsorbed on the surface of nanosheets (see Figure S1 in the Supporting Information, for example).

Table 1. Specific Surface Areas and Band Gaps of $HCa_{2-x}Sr_xNb_3O_{10}$ and $HCa_2Nb_{3-y}Ta_yO_{10}$ Nanosheet Aggregates

nanosheet	specific surface area[a]/m^2 g^{-1}	band gap[b]/eV	conduction band potential (E_{CB})[c]/V vs Ag/$AgNO_3$
$HCa_2Nb_3O_{10}$	48	3.59	−1.13
$HCa_{1.5}Sr_{0.5}Nb_3O_{10}$	47	3.55	−1.11
$HCaSrNb_3O_{10}$	58	3.50	−1.08
$HCa_{0.5}Sr_{1.5}Nb_3O_{10}$	50	3.46	−1.06
$HSr_2Nb_3O_{10}$	65	3.40	−1.03
$HCa_2Nb_{2.7}Ta_{0.3}O_{10}$	48	3.65	−1.16
$HCa_2Nb_{1.5}Ta_{1.5}O_{10}$	29	3.80	−1.23

[a]From ref 37. [b]Estimated on the basis of the onset wavelength of diffuse reflectance spectra. [c]Estimated from the empirical correlation between the conduction band potential (E_{CB}) of metal oxide semiconductors containing d^0 and d^{10} metal ions and the band gaps (E_g): E_{CB}(V vs NHE) ≈ 1.23 − E_g/2, which has been reported by Matsumoto (*J. Solid State Chem.* **1996**, *126*, 227–234). [$Ag/AgNO_3$] = [NHE] − 0.56.

Figure 2 shows UV–visible diffuse reflectance spectra of $HCa_2Nb_3O_{10}$ nanosheet aggregates modified with Pt and/or Ru–CH_3. As reported previously, the unmodified nanosheet sample does not show any absorption band in the visible light region (λ >400 nm). With modification by Pt nanoparticles, the background level rose to some extent, due to the metallic nature of Pt. Further modification of this material with Ru–CH_3 resulted in the generation of a new absorption band centered at around 460 nm, which is due to the metal-to-ligand charge transfer (MLCT) transition of Ru–CH_3. Under visible light irradiation, only the Ru complex is excited to be the ^{3}MLCT excited state, inducing electron injection to the conduction band of restacked $HCa_2Nb_3O_{10}$ nanosheets. XRD analysis showed that the interlayer d spacing of the original nanosheet sample remained almost unchanged, even upon modification of the Ru(II) complex (Figure S2 in the Supporting Information). This spacing indicates that the Ru(II) complexes underwent adsorption on the external surface of Pt/$HCa_{2-x}Sr_xNb_3O_{10}$, not intercalation into the gallery space.

2.2. H_2 Evolution on $HCa_2Nb_3O_{10}$ Nanosheets Sensitized by Different Ru(II) Complexes. We first examined the photocatalytic activities of Pt/$HCa_2Nb_3O_{10}$ nanosheets modified with different Ru(II) sensitizers. It was confirmed by control experiments that Pt/$HCa_2Nb_3O_{10}$, Ru(II) sensitizer, and EDTA were all needed for appreciable H_2 evolution. As shown in Figure 3, Pt/$HCa_2Nb_3O_{10}$ nanosheets modified with Ru–CH_3 or Ru–H produced H_2 upon visible light, and the amount of H_2 increased with time. In contrast, the use of Ru–CF_3 yielded a very low level of H_2 evolution. The turnover numbers based on the amount of adsorbed Ru sensitizers (0.2 μmol) for 5 h of visible light irradiation were calculated to be 1550, 960, and 12 for Ru–CH_3, Ru–H, and Ru–CF_3, respectively, confirming the catalytic cycle of these reactions.

2.3. H_2 Evolution Activities of $HCa_{2-x}Sr_xNb_3O_{10}$ and $HCa_2Nb_{3-y}Ta_yO_{10}$ Nanosheets Sensitized by Ru–CH_3. As shown in Figure 4, Sr-substituted $HCa_2Nb_3O_{10}$ (i.e., $HCa_{2-x}Sr_xNb_3O_{10}$) sensitized by Ru–CH_3 exhibited activity for visible-light H_2 evolution, but the H_2 evolution rate was decreased with increasing the concentration of Sr in $HCa_{2-x}Sr_xNb_3O_{10}$. Similarly, Figure 5 shows that substitution of Nb in $HCa_2Nb_3O_{10}$ for Ta tended to yield an activity drop. Consequently, $HCa_2Nb_3O_{10}$ achieved the highest performance

DOI: 10.1021/acscatal.5b00040
ACS Catal. 2015, 5, 1700–1707

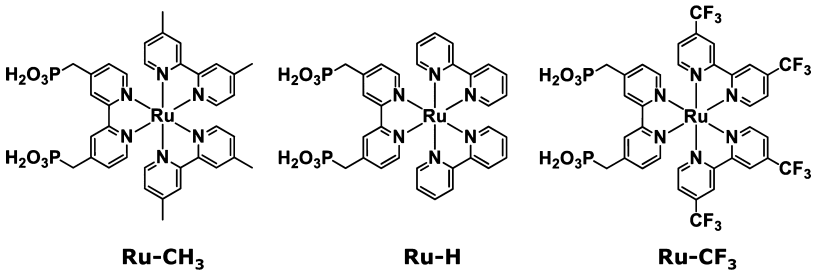

Figure 1. Ru(II) complexes employed as visible-light-sensitizers in this study.

Table 2. Spectroscopic and Electrochemical Properties of Ruthenium Complexes

	MLCT absorption band in acetonitrile		potential[a]/V		
Ru complex	λ_{max}/nm	abs coeff/M^{-1} cm^{-1}	E_{ox}	E_{ox}*[b]	E_{00}[b]
Ru−CH_3	460	15200	0.80	−1.18	1.98
Ru−H	455	15700	0.91	−1.08	1.99
Ru−CF_3	481	12700	1.21	−0.67	1.88

[a]Vs Ag/$AgNO_3$. [b]The oxidation potential of the excited state of a metal complex (E_{ox}*) is calculated using the equation $E^*_{ox} = E_{ox} - E_{00}$ according to the Franck−Condon analysis. This method is widely used to afford E^*_{ox} and estimate the driving force of electron transfer from complexes in excited state to conduction band of semiconductors (see for example: Katoh, R., et al. *J. Phys. Chem. B* **2002**, *106*, 12957−12964 and Hanson, K., et al. *J. Phys. Chem. C* **2012**, *116*, 14837−14847).

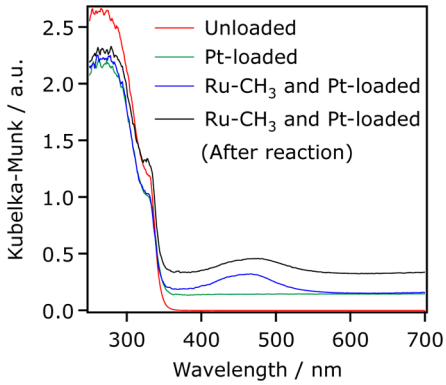

Figure 2. UV−visible diffuse reflectance spectra of $HCa_2Nb_3O_{10}$ nanosheet aggregates with various modifications.

as the building block for H_2 evolution sensitized by Ru−CH_3 with visible light among perovskite nanosheets examined.

An action spectrum of H_2 evolution on Pt/$HCa_2Nb_3O_{10}$ sensitized by Ru−CH_3 is displayed in Figure 6, along with an absorption spectrum of Ru−CH_3. The change in apparent quantum yield corresponds well to that in the absorption spectrum, and the longest wavelength available for the reaction is 550 nm. Under 600 nm irradiation, no H_2 evolution occurred. These results indicate that the observed H_2 evolution was initiated by excitation of Ru−CH_3. The maximum apparent quantum yield obtained was ca. 10% at 460 nm.[38]

As shown in Figure S4 in the Supporting Information, the amount of H_2 was increased with time, reaching a steady production rate after 3−4 h of irradiation. While prolonged reaction resulted in a slight drop in activity, the turnover number of H_2 evolution with respect to the amount of the adsorbed Ru−CH_3 was approximately 3800. The induction period is likely to be due to the reduction of electron-deficient

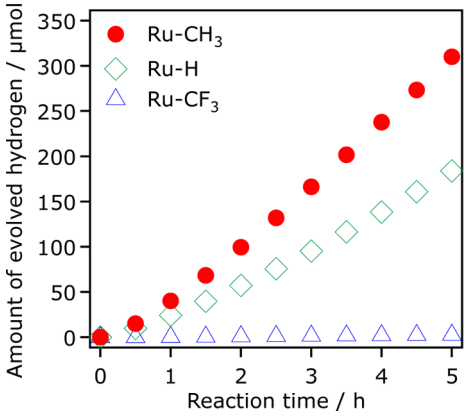

Figure 3. Time courses of H_2 evolution on Pt-loaded $HCa_2Nb_3O_{10}$ nanosheets sensitized by different Ru(II) complexes under visible light (λ = 420 nm). Reaction conditions: catalyst, 25 mg; aqueous solution containing 10 mM EDTA (100 mL); light source, xenon lamp (300 W) with a band-pass filter.

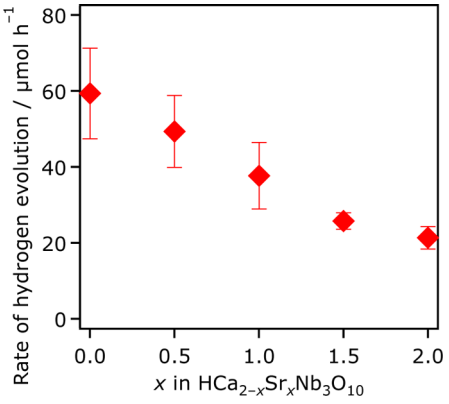

Figure 4. Dependence of the rate of H_2 evolution on Pt-loaded $HCa_{2-x}Sr_xNb_3O_{10}$ nanosheets sensitized by Ru−CH_3 under visible light (λ = 420 nm) on the compositional parameter (x). Reaction conditions: catalyst, 25 mg; aqueous solution containing 10 mM EDTA (100 mL); light source, xenon lamp (300 W) with a band-pass filter.

Pt nanoparticles by photogenerated electrons. In fact, a UV−visible diffuse reflectance spectrum of the reacted sample showed a more pronounced background level (Figure 2), which means an increased density of metallic Pt. The MLCT absorption band was still observed even after 20 h of photocatalytic reaction, but the intensity was slightly decreased, indicative of the decomposition of Ru during the reaction to a certain extent.

2.4. Photoelectrochemical Measurements. We have previously reported that the activity of $HCa_2Nb_3O_{10}$ nanosheet

DOI: 10.1021/acscatal.5b00040
ACS Catal. 2015, 5, 1700−1707

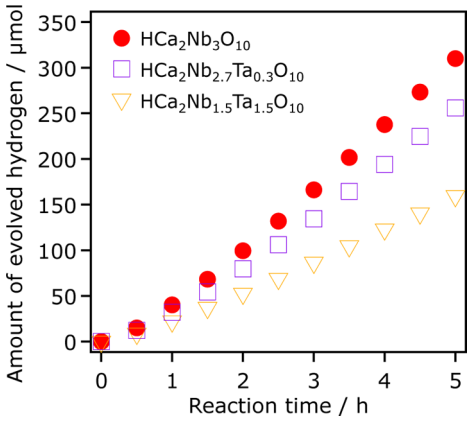

Figure 5. Time courses of H_2 evolution on Pt-loaded $HCa_2Nb_{3-y}Ta_yO_{10}$ nanosheets sensitized by Ru−CH_3 under visible light (λ = 420 nm). Reaction conditions: catalyst, 25 mg; aqueous solution containing 10 mM EDTA (100 mL); light source, xenon lamp (300 W) with a band-pass filter.

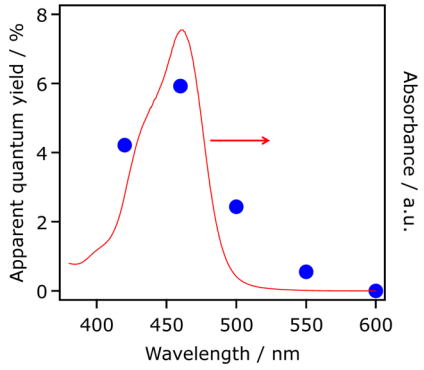

Figure 6. Action spectrum of H_2 evolution on Pt-loaded $HCa_2Nb_3O_{10}$ nanosheets sensitized by Ru−CH_3 under visible light. Reaction conditions: catalyst, 25 mg; aqueous solution containing 10 mM EDTA (100 mL); light source, xenon lamp (300 W) with a band-pass filter. The total number of incident photons was fixed to be ca. 12 mW.

aggregates sensitized by $Ru^{II}(bpy)_3$ or $Ru^{II}\{(bpy)_2(4,4'\text{-}(PO_3H_2)_2bpy)\}$ for H_2 evolution is primarily governed by the electron injection efficiency from the excited-state Ru(II) sensitizer to the conduction band of the nanosheet.[21,22] In this study, we assessed relative electron injection efficiencies by means of a photoelectrochemical technique using porous electrodes of $Ca_{2-x}Sr_xNb_3O_{10}^-$ and $Ca_2Nb_{3-y}Ta_yO_{10}^-$ nanosheets modified with a Ru(II) complex. As described in the Experimental Section, the electrodes were prepared by pasting a vigorous slurry of a given nanosheet aggregates onto a FTO conductive glass, followed by calcination in air at 723 K for 1 h and immobilization of Ru(II) sensitizers. In order to avoid topochemical dehydration of $HCa_2Nb_3O_{10}$ that occurs irreversibly at 463−573 K,[39] TBA^+-exfoliated nanosheets were reassembled by K^+ ions upon reaction with an aqueous KOH solution.

Figure 7A shows current−voltage curves for the prepared $KCa_2Nb_3O_{10}$ electrodes sensitized by three Ru(II) complexes under intermittent visible light (λ >420 nm) in an aqueous solution containing 10 mM EDTA and 0.1 M Na_2SO_4. The working principle of this photoelectrochemical system is identical with that of the water-splitting solar cell developed by Mallouk et al.[40] Briefly, the adsorbed Ru(II) complex undergoes photoexcitation upon visible light, injecting electrons into the conduction band of a semiconductor. The oxidized state of the Ru(II) complex is reduced by reaction with an electron-donating species (here, EDTA) to regenerate the Ru component. The injected electrons pass through an external circuit to reach a counter electrode (here a Pt wire), finally reducing H^+ into H_2. The $KCa_2Nb_3O_{10}$ electrode alone (without Ru) exhibited little photocurrent due to the large band gap (3.59 eV) that is unable to absorb visible light (Figure S5 in the Supporting Information). However, electrodes that were sensitized by Ru−CH_3 or Ru−H generated anodic photocurrent upon visible light, indicating that electron injection occurred from the excited-state Ru(II) sensitizers to the conduction band of $KCa_2Nb_3O_{10}$. In contrast, the Ru−CF_3 electrode did not show appreciable photocurrent in the entire potential range examined. Similarly, photoelectrochemical properties of $KCa_{2-x}Sr_xNb_3O_{10}$ and $KCa_2Nb_{3-y}Ta_yO_{10}$ nanosheets sensitized by Ru−CH_3 were examined. As shown in Figure 7B, $KCa_{2-x}Sr_xNb_3O_{10}$ electrodes exhibited anodic photoresponse, giving a similar level of photocurrent (15−20

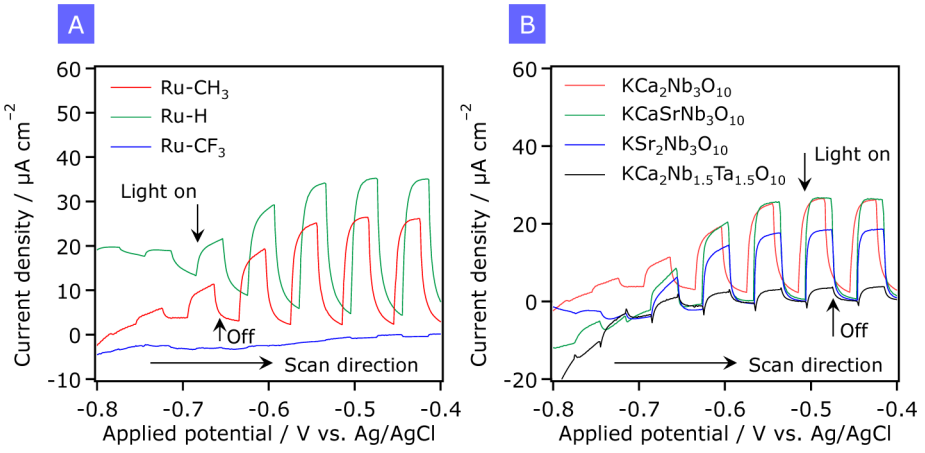

Figure 7. Current−voltage curves for porous electrodes of $KCa_{2-x}Sr_xNb_3O_{10}$ and $KCa_2Nb_{3-y}Ta_yO_{10}$ nanosheets (5.25 cm^2) sensitized by Ru(II) complexes in aqueous 0.1 M Na_2SO_4 solution containing 10 mM EDTA under intermittent visible light irradiation (λ >420 nm): (A) $KCa_2Nb_3O_{10}$ sensitized by different Ru(II) complexes (an enlarged view of the Ru−CF_3 data is shown in Figure S5 in the Supporting Information); (B) $KCa_{2-x}Sr_xNb_3O_{10}$ and $KCa_2Nb_{3-y}Ta_yO_{10}$ sensitized by Ru−CH_3. Scan rate: 10 mV s^{-1}.

DOI: 10.1021/acscatal.5b00040
ACS Catal. 2015, 5, 1700−1707

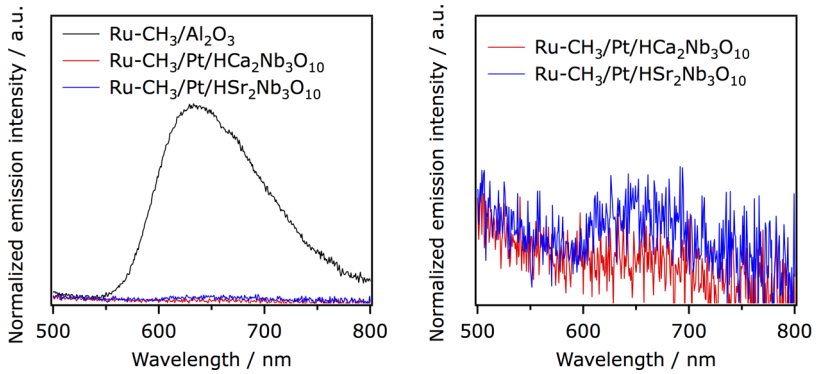

Figure 8. Steady-state emission spectra for Pt-loaded $HCa_{2-x}Sr_xNb_3O_{10}$ nanosheets sensitized by Ru−CH_3 with 444 nm excitation, along with that of Ru−CH_3/Al_2O_3 for reference. The spectra were acquired at room temperature under an Ar atmosphere using aqueous EDTA solution (10 mM, 3.0 mL) containing 0.5 wt % Pt-loaded $HCa_{2-x}Sr_xNb_3O_{10}$ (5.0 mg) adsorbed with Ru−CH_3 (8.0 μmol g^{-1}). The right panel indicates an enlarged view of the left panel. Note that the ^{3}MLCT excited state of Ru−CH_3 does not undergo reductive quenching in the presence of EDTA.

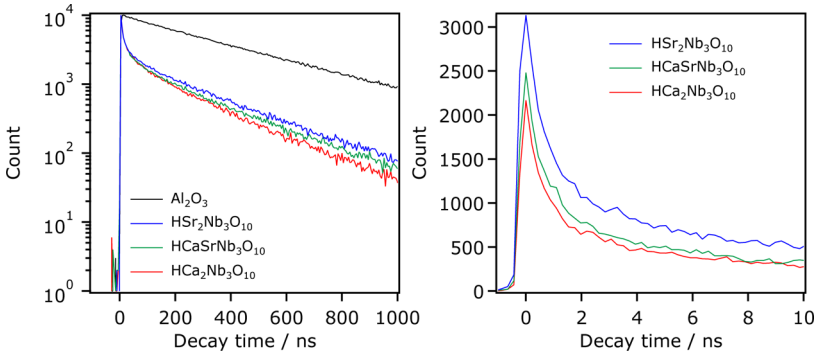

Figure 9. Emission decay profiles of Ru−CH_3/Pt/$HCa_{2-x}Sr_xNb_3O_{10}$ nanosheets excited at 444 nm and monitored at 630 nm. The tested suspensions were prepared in the same manner as described in the caption of Figure 8. As a reference, data for Ru−CH_3/Al_2O_3 is also shown. In the left panel, for each sample, the measurement was repeated until the signal count just after the photoexcitation (at t = 0) reached 10^4. In the right panel, each measurement was conducted by irradiating the sample cell with a fixed number of photons.

μA cm^{-2}) to each other. On the other hand, substitution of Nb in $KCa_2Nb_3O_{10}$ for Ta resulted in a significant drop in photocurrent. Thus, photoresponse of a Ru(II) complex/nanosheet electrode was shown to depend strongly on the adsorbed Ru(II) complex as well as the composition of the nanosheet.

2.5. Factors Affecting Photocatalytic Hydrogen Evolution Activity. The results of photocatalytic H_2 evolution using $HCa_{2-x}Sr_xNb_3O_{10}$ and $HCa_2Nb_{3-y}Ta_yO_{10}$ nanosheets sensitized by Ru(II) complexes indicated that the activities were influenced by both the structure of the Ru(II) complex and the nanosheet composition. The oxidation potential of the ^{3}MLCT excited state of the Ru(II) complexes (E_{ox}*) calculated according to the Franck−Condon analysis shifted positively in the order of Ru−CH_3, Ru−H, and Ru−CF_3, as shown in Table 2. The results of photoelectrochemical measurements using the different Ru(II) complexes and the restacked $HCa_2Nb_3O_{10}$ nanosheets (Figure 7A), which showed the lowest performance of the Ru−CF_3 electrode, could be explained in terms of the much more positively shifted E_{ox}* value, in comparison to those for the other complexes. As given in Table 1, the E_{CB} value of $HCa_2Nb_3O_{10}$ nanosheets was found to be too negative for these nanosheets to accept electrons from the ^{3}MLCT excited state of Ru−CF_3.

According to the same idea, one can expect that a larger difference between the oxidation potential of the ^{3}MLCT excited state (E_{ox}*) of a Ru(II) sensitizer and the E_{CB} of a nanosheet will contribute to more efficient electron injection, resulting in an enhanced photocatalytic H_2 evolution, while a smaller difference will not. As given in Table 1, the E_{CB} value of $HCa_{2-x}Sr_xNb_3O_{10}$ nanosheets shifts positively with an increase in the Sr content, while that of $HCa_2Nb_{3-y}Ta_yO_{10}$ nanosheets shifts negatively with an increase in the Ta content. The decrease in activity with an increase in the Ta content in $HCa_2Nb_{3-y}Ta_yO_{10}$ (Figure 5) can be explained in terms of the reduced driving force for the electron injection, as observed in the photoelectrochemical measurements (Figure 7B). Interestingly, however, the negatively shifted E_{CB} of Sr-rich $HCa_{2-x}Sr_xNb_3O_{10}$ has no positive impact on the electron injection event and the resulting H_2 evolution activity, in comparison to $HCa_2Nb_3O_{10}$ (Figures 4 and 7B).

The efficiency of electron injection from the excited state of Ru−CH_3 to the conduction band of a nanosheet was also examined by mean of steady-state emission spectroscopy. It is known that emission of Ru(II) polypyridyl complexes is quenched in the presence of a semiconductor, as a result of electron injection into the conduction band.[21,22] We thus measured absolute emission quantum yields of Ru−CH_3 adsorbed on $HCa_{2-x}Sr_xNb_3O_{10}$ under conditions identical with those for the photocatalytic reaction but with 444 nm light that is selectively absorbed by Ru−CH_3 (see Figure 2).[41] Ru−CH_3 on Al_2O_3, which is an insulator, showed an emission peak centered at around 630 nm (Figure 8), giving an emission quantum yield of ca. 5.6%. In contrast, we observed a

DOI: 10.1021/acscatal.5b00040
ACS Catal. 2015, 5, 1700−1707

substantial drop in the emission intensity in the presence of Pt-loaded $HCa_{2-x}Sr_xNb_3O_{10}$, with only <1% emission quantum yields, regardless of the Sr content. This efficient quenching indicates that most of the excited state of Ru−CH_3 contributed to the electron injection event regardless of the composition of nanosheet material, in good agreement with the result of photoelectrochemical measurements (Figure 7). Note that these experiments assessed the electron injection process not only from the ^{3}MLCT excited state but also from ^{1}MLCT, which is known to be an ultrafast process that occurs within a time scale of several hundreds of femtoseconds.[42,43]

To further obtain more insight into the electron injection process, we measured the decay curves of emission from Ru−CH_3 adsorbed on Pt/$HCa_{2-x}Sr_xNb_3O_{10}$ and Al_2O_3.[44] Here, due to the time resolution of our apparatus (>0.2 ns), the observed emission decay is attributed largely to emission from the lowest ^{3}MLCT excited state.[45] As shown in Figure 9, the emission decay of the Sr material was relatively slow, but the Ca-containing material showed faster decay profiles. The slower emission decay of the Sr material indicates slower electron injection. It is notable that there is a fast decay component on a time scale of shorter than 2 ns, suggesting relatively fast electron injection that possibly occurred during the relaxation process from the singlet to triplet MLCT excited state.

The decay profiles of the $HCa_{2-x}Sr_xNb_3O_{10}$ samples could be resolved using three components (Table S1 in the Supporting Information), suggesting that there were different adsorption forms of Ru−CH_3 on the $HCa_{2-x}Sr_xNb_3O_{10}$ surface. As reported previously, the restacked $HCa_{2-x}Sr_xNb_3O_{10}$ nanosheets consist of aggregated sheets with highly disordered structures.[37] Therefore, it would be reasonable to assume that adsorption sites are different from each other.

The slower electron injection of the Sr material in comparison to that of the Ca-containing material may seem unreasonable, because one can expect an increased driving force for electron injection due to the enlarged difference between E_{ox}* and E_{CB} with an increase in the Sr content. One possible explanation for this is that part of the electrons from the excited state of Ru−CH_3 are injected not only into the conduction band of $HCa_{2-x}Sr_xNb_3O_{10}$ nanosheets but also into surface trapping states in the material.[42,43] Although we do not have any measures to evaluate such surface states existing in $HCa_{2-x}Sr_xNb_3O_{10}$, it is known that in an n-type semiconductor such as the present niobates, surface states are located below the conduction band.[43] In particular, the highly disordered surface of $HCa_{2-x}Sr_xNb_3O_{10}$ nanosheets could offer many defects that give localized states working as electron-accepting levels. With an increase in the concentration of Ca in $HCa_{2-x}Sr_xNb_3O_{10}$, the distortion of the triple-layer perovskite blocks in the material is more pronounced.[28,37] This situation may cause the generation of more vacancies and increased number of surface states, contributing to more efficient electron injection from the excited state of Ru−CH_3. So far, several researchers have pointed out the important role of surface states as electron acceptors in the primary process of dye-sensitized solar cells.[42,43] Grätzel et al. observed ultrafast electron injection from the S1 state of alizarin dye to ZrO_2, despite the fact that the E_{CB} of ZrO_2 lies ∼1 eV above the singlet excited state of alizarin.[42] Furube et al. have reported that electron injection from *cis*-bis(4,4′-dicarboxy-2,2′-bipyridine)dithiocyanatoruthenium(II), so-called N3 dye, to ZnO occurs via a surface trapping state.[43]

On consideration of these results, a plausible explanation for the activity drop observed in Sr-rich $HCa_{2-x}Sr_xNb_3O_{10}$ nanosheets (Figure 4) is that the ability of conduction band electrons to reduce protons into H_2 is lowered due to the positive shift of the E_{CB} value. This idea could also explain the difference in H_2 evolution activity of $HCa_{2-x}Sr_xNb_3O_{10}$ nanosheets under band gap irradiation. As we have reported previously, the rate of H_2 evolution on Pt-loaded $HCa_{2-x}Sr_xNb_3O_{10}$ nanosheets under 300 nm irradiation decreased with an increase in the Sr content.[37] This in turn implies that the rate-determining step for the sensitized H_2 evolution using $HCa_{2-x}Sr_xNb_3O_{10}$ nanosheets is the electron transfer process from the conduction band to the loaded Pt. When Nb in $HCa_2Nb_3O_{10}$ was replaced by Ta, on the other hand, the electron injection process from the excited-state Ru−CH_3 to the nanosheets would be rate determining.

It was thus elucidated that a semiconductor material with a suitable E_{CB}, which maximizes electron injection efficiency from the excited-state sensitizer and minimizes the loss of the water reduction driving force, is required for efficient dye-sensitized H_2 evolution. In addition to the E_{CB} value, surface states in a semiconductor are suggested to affect the performance, as they could work as electron traps from excited-state photosensitizers. The water-splitting system based on dye sensitization has recently been extended to nonsacrificial schemes such as dye-sensitized water-splitting solar cells[40] and Z-scheme water splitting using two different semiconductors.[24] We believe that the findings of the present study will give useful information for the development of those systems.

3. CONCLUSION

H_2 evolution activities of $HCa_{2-x}Sr_xNb_3O_{10}$ and $HCa_2Nb_{3-y}Ta_yO_{10}$ nanosheets sensitized by Ru(II) polypyridyl complexes were examined. The E_{CB} values of $HCa_{2-x}Sr_xNb_3O_{10}$ and $HCa_2Nb_{3-y}Ta_yO_{10}$ nanosheets have a significant impact on the activity, as it determines the reactivity of conduction band electrons and the efficiency of electron injection from the excited-state sensitizer. A semiconductor material that has a conduction band potential suitable for both electron injection from the excited-state sensitizer and the reduction of protons is thus shown to be essential for efficient visible-light H_2 evolution sensitized by a Ru(II) polypyridyl complex. The results of emission spectroscopy also implied that surface states existing in Ca-rich $HCa_{2-x}Sr_xNb_3O_{10}$ nanosheets might play an important role in accepting electrons from the excited-state sensitizer and promoting the water reduction reaction.

4. EXPERIMENTAL SECTION

4.1. Preparation of Restacked $HCa_{2-x}Sr_xNb_3O_{10}$ and $HCa_2Nb_{3-y}Ta_yO_{10}$ Nanosheets. The detailed procedure can be found in our previous paper, which also includes the results of structural characterization.[37] Briefly, a layered solid was subject to proton exchange with HNO_3, followed by reaction with TBAOH to exfoliate the layered structure. The resulting colloidal sheets were reassembled by adding HCl. The as-prepared materials were employed as building blocks for dye-sensitized H_2 evolution. For use as a photoanode material, the nanosheet suspension was precipitated by KOH.

4.2. Modification with Nanoparticulate Platinum. Before photocatalytic reactions, the as-prepared nanosheet aggregates were modified with nanoparticulate Pt as a cocatalyst by an in situ photodeposition method.[46] The photodeposition experiment was conducted in a closed gas circulation system made of glass, similar to the photocatalytic reaction system described below. The powdered

DOI: 10.1021/acscatal.5b00040
ACS Catal. 2015, 5, 1700−1707

nanosheet sample was first dispersed in an aqueous methanol solution (10 vol %, 100 mL) containing an appropriate amount of $H_2PtCl_6 \cdot 2H_2O$ (Kanto Chemicals, 97% Pt) as the source of Pt, using a magnetic stirrer. After mixing, the solution was evacuated to completely remove dissolved air and then irradiated with UV light (λ >300 nm) for 2 h using a 300 W xenon lamp (Cermax, PE300BF) with an output current of 20 A. The resulting powder was filtered and washed with pure water, followed by drying in an oven at 343 K overnight. The amount of Pt loaded was 0.5 wt % as the metallic basis.

4.3. Preparation of Electrodes. Porous electrodes made of KOH-restacked nanosheets were prepared by a conventional squeegee method. First, a mixture of 50 mg of a nanosheet solid, 10 μL of acetyl acetone (Kanto Chemicals), 10 μL of Triton X (Aldrich, USA), 10 μL of poly(ethylene glycol) 300 (Kanto Chemicals), and 500 μL of distilled water was ground in an agate mortar to prepare the viscous slurry. The slurry was then pasted onto fluorine-doped tin oxide (FTO) glass slides (thickness 1.8 mm; Asahi Glass, Japan) to prepare 1.5 × 3.5 cm^2 electrodes. The electrode samples were subsequently calcined in air at 723 K for 1 h.

4.4. Adsorption of Ru(II) Complexes. The HCl-restacked nanosheets (50 mg) modified with Pt were suspended in acetonitrile containing a Ru(II) complex (total volume, 10 mL). After it was stirred magnetically overnight in the dark, the suspension was filtered, and the resulting dark orange powder was collected. Finally, the collected powder was dried in an oven at 343 K overnight. For electrode materials, a nanosheet/FTO electrode was immersed in 25 mL of acetonitrile containing 10 nmol of a Ru(II) complex. The solution was stirred magnetically in the dark overnight. The amount of adsorbed Ru(II) sensitizers onto a given substrate was estimated by using the equation

$$\text{adsorbed amount } (\mu\text{mol g}^{-1}) = \frac{A_{\text{before}} - A_{\text{after}}}{A_{\text{before}}} \frac{C\ (\mu\text{mol L}^{-1}) \times 10 \times 10^{-3}\ (\text{L})}{50 \times 10^{-3}\ (\text{g})}$$

where A_{before} and A_{after} indicate the absorbance of a given Ru(II) complex in a test solution at the ^{3}MLCT maximum wavelength before and after the adsorption procedure and C is the concentration of the complex in the solution before adsorption, respectively.

The complexes $Ru\{(4,4'\text{-}X_2\text{-bpy})_2(4,4'\text{-}(CH_2PO_3H_2)_2\text{-bpy})\}(PF_6)_2$ (X = H, CH_3, CF_3; bpy = 2,2′-bipyridine) were synthesized according to the previous literature methods with some modifications.[47,48] It was confirmed by ^{1}H NMR spectroscopy, electrospray ionization mass-spectroscopy (ESI-MS), and elemental analysis that the complexes were successfully synthesized.

4.5. Hydrogen Evolution Reactions. Reactions were carried out in a Pyrex top-irradiation vessel connected to a glass closed gas circulation system, as described in a previous paper.[49] A 25 mg sample of Ru-adsorbed sample was dispersed in an aqueous EDTA solution (10 mM, 100 mL, pH ~5.5) using a magnetic stirrer, and this reactant solution was evacuated under vacuum several times to completely remove any residual air. Then, a small amount of Ar gas (ca. 5 kPa) was introduced into the reaction system prior to irradiation under a 300 W xenon lamp (Cermax, PE300BF) with an output current of 20 A. The irradiation wavelength was controlled by a cold mirror, cutoff filter, band-pass filter, and water filter (λ = 420 nm). The reactant solution was maintained at room temperature by a water bath during the reaction. The evolved gases were analyzed by gas chromatography (Shimadzu, GC-8A with TCD detector and MS-5A column, argon carrier gas).

The apparent quantum yield (AQY) for H_2 evolution was measured using the same experimental setup but with another xenon lamp (Asahi Spectra, MAX-303), and was estimated as

$$\text{AQY } (\%) = (A \times R/I) \times 100$$

where A, R, and I represent the coefficient based on the reaction (H_2 evolution, 1), the H_2 evolution rate, and the rate of incident photons, respectively. Here we assume that one electron is required to produce one H_2 molecule, because of a possible current doubling effect (as we discussed in our previous paper).[21,50] The total number of incident photons (ca. 12 mW) was measured using a calibrated silicon photodiode. To obtain an action spectrum, we used different band-pass filters.

4.6. Photoelectrochemical Measurements. Photoelectrochemical measurements were carried out using a potentiostat (HSV-110, Hokuto Denko) and a conventional electrochemical cell at room temperature. The cell was made of Pyrex glass and consisted of a three electrode-type system using a Pt wire and an Ag/AgCl electrode as the counter and reference electrodes, respectively. An aqueous Na_2SO_4 solution (0.1 M) containing the EDTA salt (10 mM) was employed as the electrolyte and was saturated with argon gas prior to the electrochemical measurements. The light source was a 300 W xenon lamp (Cermax, PE300BF) fitted with a cold mirror and a cutoff filter (λ >420 nm).

■ ASSOCIATED CONTENT

Supporting Information

The following file is available free of charge on the ACS Publications website at DOI: 10.1021/acscatal.5b00040.

UV−visible absorption spectra, X-ray diffraction patterns, H_2 evolution, photoelectrochemical data, and emission lifetime data (PDF)

■ AUTHOR INFORMATION

Corresponding Author

*K.M.: e-mail, maedak@chem.titech.ac.jp; fax, +81-3-5734-2284; tel, +81-3-5734-2239.

Present Address

∥(For M.E.) Electronic Functional Materials Group, Polymer Materials Unit, National Institute for Materials Science, 1-1 Namiki, Tsukuba, Ibaraki 305-0044, Japan.

Notes

The authors declare no competing financial interest.

■ ACKNOWLEDGMENTS

This work was supported by the ENEOS Hydrogen Trust Fund, Grant-in-Aid for Scientific Research on Innovative Areas (Project No. 25107512; AnApple), and the PRESTO/JST program "Chemical Conversion of Light Energy". The authors thank Mr. Yutaro Ueda and Ms. Ayako Suzuki for assistance in emission measurements.

■ REFERENCES

(1) Maeda, K.; Domen, K. *J. Phys. Chem. C* **2007**, *111*, 7851−7861.
(2) Kudo, A.; Miseki, Y. *Chem. Soc. Rev.* **2009**, *38*, 235−278.
(3) Youngblood, W. J.; Lee, S.-H. A.; Maeda, K.; Mallouk, T. E. *Acc. Chem. Res.* **2009**, *42*, 1966−1973.
(4) Abe, R. *J. Photochem. Photobiol. C* **2010**, *11*, 179−209.
(5) Maeda, K. *J. Photochem. Photobiol. C* **2011**, *12*, 237−268.
(6) Osterloh, F. E. *Chem. Soc. Rev.* **2013**, *42*, 2294−2320.
(7) Wen, F.; Li, C. *Acc. Chem. Res.* **2013**, *46*, 2355−2364.
(8) Houlding, V. H.; Grätzel, M. *J. Am. Chem. Soc.* **1983**, *105*, 5695−5696.
(9) Shimizu, T.; Iyoda, T.; Koide, Y. *J. Am. Chem. Soc.* **1985**, *107*, 35−41.
(10) Furlong, D. N.; Wells, D.; Sasse, W. H. F. *J. Phys. Chem.* **1986**, *90*, 1107−1115.
(11) Kim, Y. I.; Salim, S.; Huq, M. J.; Mallouk, T. E. *J. Am. Chem. Soc.* **1991**, *113*, 9561−9563.
(12) Hirano, K.; Suzuki, E.; Ishikawa, A.; Moroi, T.; Shiroishi, H.; Kaneko, M. *J. Photochem. Photobiol., A* **2000**, *136*, 157−161.
(13) Abe, R.; Hara, K.; Sayama, K.; Domen, K.; Arakawa, H. *J. Photochem. Photobiol., A* **2000**, *137*, 63−69.

DOI: 10.1021/acscatal.5b00040
ACS Catal. 2015, 5, 1700−1707

(14) Ikeda, S.; Abe, C.; Torimoto, T.; Ohtani, B. *J. Photochem. Photobiol., A* **2003**, *160*, 61−67.
(15) Bae, E.; Choi, W.; Park, J.; Shin, H. S.; Kim, S. B.; Lee, J. S. *J. Phys. Chem. B* **2004**, *108*, 14093−14101.
(16) Bae, E.; Choi, W. *J. Phys. Chem. B* **2006**, *110*, 14792−14729.
(17) Park, H.; Choi, W. *Langmuir* **2006**, *22*, 2906−2911.
(18) Li, Q.; Jin, Z.; Peng, Z.; Li, Y.; Li, S.; Lu, G. *J. Phys. Chem. C* **2007**, *111*, 8237−8241.
(19) Li, Q.; Chen, L.; Lu, G. *J. Phys. Chem. C* **2007**, *111*, 11494−11499.
(20) Maeda, K.; Eguchi, M.; Youngblood, W. J.; Mallouk, T. E. *Chem. Mater.* **2008**, *20*, 6770−6778.
(21) Maeda, K.; Eguchi, M.; Lee, S.-H. A.; Youngblood, W. J.; Hata, H.; Mallouk, T. E. *J. Phys. Chem. C* **2009**, *113*, 7962−7969.
(22) Maeda, K.; Eguchi, M.; Youngblood, W. J.; Mallouk, T. E. *Chem. Mater.* **2009**, *21*, 3611−3617.
(23) Reisner, E.; Fontecilla-Camps, J. C.; Armstrong, F. A. *Chem. Commun.* **2009**, 550−552.
(24) Abe, R.; Shinmei, K.; Hara, K.; Ohtani, B. *Chem. Commun.* **2009**, 3577−3579.
(25) Takanabe, K.; Kamata, K.; Wang, X.; Antonietti, M.; Kubota, J.; Domen, K. *Phys. Chem. Chem. Phys.* **2010**, *12*, 13020−13025.
(26) Li, Q.; Che, Y.; Ji, H.; Chen, C.; Zhu, H.; Ma, W.; Zhao, J. *Phys. Chem. Chem. Phys.* **2014**, *16*, 6550−6554.
(27) Gerischer, H. *Photochem. Photobiol.* **1972**, *16*, 243−260.
(28) Treacy, M. M. J.; Rice, S. B.; Jacobson, A. J.; Lewandowski, J. T. *Chem. Mater.* **1990**, *2*, 279−286.
(29) Keller, S. W.; Kim, H.-N.; Mallouk, T. E. *J. Am. Chem. Soc.* **1994**, *116*, 8817−8818.
(30) Sasaki, T.; Watanabe, M.; Hashizume, H.; Yamada, H.; Nakazawa, H. *J. Am. Chem. Soc.* **1996**, *118*, 8329−8335.
(31) Schaak, R. E.; Mallouk, T. E. *Chem. Mater.* **2000**, *12*, 3427−3434.
(32) Ebina, Y.; Sasaki, T.; Harada, M.; Watanabe, M. *Chem. Mater.* **2002**, *14*, 4390−4395.
(33) Ida, S.; Ogata, C.; Unal, U.; Izawa, K.; Inoue, T.; Altuntasoglu, O.; Matsumoto, Y. *J. Am. Chem. Soc.* **2007**, *129*, 8956−8957.
(34) Matsumoto, Y.; Koinuma, M.; Iwanaga, Y.; Sato, T.; Ida, S. *J. Am. Chem. Soc.* **2009**, *131*, 6644−6645.
(35) Ida, S.; Okamoto, Y.; Matsuka, M.; Hagiwara, H.; Ishihara, T. *J. Am. Chem. Soc.* **2012**, *134*, 15773−15782.
(36) Oshima, T.; Ishitani, O.; Maeda, K. *Adv. Mater. Interfaces* **2014**, *1*, 1400131.
(37) Maeda, K.; Eguchi, M.; Oshima, T. *Angew. Chem., Int. Ed.* **2014**, *53*, 13164−13168.
(38) Time courses of H_2 evolution under 460 nm irradiation using different amounts of $Pt/HCa_2Nb_3O_{10}$ modified with $Ru-CH_3$ are shown in Figure S3 (see the Supporting Information). The result showed that the H_2 evolution rate underwent saturation at a catalyst mass of 50−100 mg, with a maximum AQY of ca. 10%.
(39) Fang, M.; Kim, C. H.; Mallouk, T. E. *Chem. Mater.* **1999**, *11*, 1519−1525.
(40) Youngblood, W. J.; Lee, S.-H. A.; Kobayashi, Y.; Hernandez-Pagan, E. A.; Hoertz, P. G.; Moore, T. A.; Moore, A. L.; Gust, D.; Mallouk, T. E. *J. Am. Chem. Soc.* **2009**, *131*, 926−927.
(41) Absolute emission quantum yields of $Ru-CH_3$ immobilized on the nanosheet surface were measured using a multichannel spectrometer attached to a calibrated integrating sphere (C9920-02G: Hamamatsu Photonics) with 444 nm excitation. The measurements were conducted by dispersing 5.0 mg of $Ru-CH_3/Pt/HCa_{2-x}Sr_xNb_3O_{10}$ powder in 3.0 mL of 10 mM EDTA aqueous solution under an Ar atmosphere.
(42) Huber, R.; Sebastian Spörlein, S.; Moser, J. E.; Grätzel, M.; Wachtveitl, J. *J. Phys. Chem. B* **2000**, *104*, 8995−9003.
(43) Furube, A.; Katoh, R.; Hara, K.; Murata, S.; Arakawa, H.; Tachiya, M. *J. Phys. Chem. B* **2003**, *107*, 4162−4166.
(44) Emission decay monitored at 630 nm, corresponding to the emission from $Ru-CH_3$, was measured by the time-dependent single photon counting method using a FluoroCube 1000U-S spectrofluorometer under 444 nm photoexcitation (NanoLED-440L, HORIBA) with a TBX-04 detector. A 5.0 mg portion of $Ru-CH_3/Pt/HCa_{2-x}Sr_xNb_3O_{10}$ powder was dispersed in 3.0 mL of 10 mM EDTA aqueous solution with continuous magnetic stirring under an Ar atmosphere.
(45) Yui, T.; Takeda, H.; Ueda, Y.; Sekizawa, K.; Koike, K.; Inagaki, S.; Ishitani, O. *ACS Appl. Mater. Interfaces* **2014**, *6*, 1992−1998.
(46) Kraeutler, B.; Bard, A. J. *J. Am. Chem. Soc.* **1978**, *100*, 4317−4318.
(47) Gholamkhass, B.; Mametsuka, H.; Koike, K.; Furue, M.; Ishitani, O. *Inorg. Chem.* **2005**, *44*, 2326−2336.
(48) Norris, M. R.; Concepcion, J. J.; Glasson, C. R. K.; Fang, Z.; Lapides, A. M.; Ashford, D. L.; Templeton, J. L.; Meyer, T. J. *Inorg. Chem.* **2013**, *52*, 12492−12501.
(49) Maeda, K.; Higashi, M.; Lu, D.; Abe, R.; Domen, K. *J. Am. Chem. Soc.* **2010**, *132*, 5858−5868.
(50) Matsumura, M.; Ohnishi, H.; Hanafusa, K.; Tsubomura, H. *Bull. Chem. Soc. Jpn.* **1987**, *60*, 2001−2003.

DOI: 10.1021/acscatal.5b00040
ACS Catal. 2015, 5, 1700−1707